Published in final edited form as:

Chem Res Toxicol. 2017 August 21; 30(8): 1641–1651. doi:10.1021/acs.chemrestox.7b00136.

Rapid dissolution of ZnO nanoparticles induced by biological buffers significantly impacts cytotoxicity

Josh E. Eixenberger[†,‡], **Catherine B. Anders**[†,‡], **Rebecca J. Hermann**[†], **Raquel J. Brown**[⊥], **Kongara M. Reddy**[‡], **Alex Punnoose**[‡], and **Denise G. Wingett**[*,†]

[†]Biomolecular Sciences Graduate Program, Boise State University, Boise, ID 83725, USA

[‡]Department of Physics, Boise State University, Boise, ID 83725, USA

[⊥]Biomolecular Research Center, Boise State University, Boise, ID 83725, USA

Abstract

Zinc oxide nanoparticles (nZnO) are one of the most highly produced nanomaterials and are used in numerous applications including cosmetics and sunscreens despite reports demonstrating their cytotoxicity. Dissolution is viewed as one of the main sources of nanoparticle (NP) toxicity, however dissolution studies can be time-intensive to perform and complicated by issues such as particle separation from solution. Our work attempts to overcome some of these challenges by utilizing new methods using UV/vis and fluorescence spectroscopy to quantitatively assess nZnO dissolution in various biologically relevant solutions. All biological buffers tested induce rapid dissolution of nZnO. These buffers, including HEPES, MOPS, and PIPES, are commonly used in cell culture media, cellular imaging solutions and to maintain physiological pH. Additional studies using X-ray diffraction, FT-IR, X-ray photoelectron spectroscopy, ICP-MS and TEM were performed to understand how the inclusion of these non-essential media components impacts the behavior of nZnO in RPMI media. From these assessments, we demonstrate that HEPES causes increased dissolution kinetics, boosts the conversion of nZnO into zinc phosphate/carbonate and, interestingly, alters the structural morphology of the complex precipitates formed with nZnO in cell culture conditions. Cell viability experiments demonstrated that the inclusion of these buffers significantly decreases the viability of Jurkat leukemic cells when challenged with nZnO. This work demonstrates that biologically relevant buffering systems dramatically impact the dynamics of nZnO including dissolution kinetics, morphology, complex precipitate formation, and toxicity profiles.

Graphical abstract

[*]**Corresponding Author** Denise Wingett, Boise State University, 1910 W. University Dr., Boise, ID 83725. Fax: 208-392-1430. Phone number: 208-426-2921. denisewingett@boisestate.edu.
Current Address: 1910 W. University Dr., Boise, ID 83725. Fax: 208-392-1430. Phone number: 208-426-2921

ASSOCIATED CONTENT

Supporting Information. UV/vis and spectrofluorometric monitoring of dissolution, Cellular media component screening, X-ray diffraction, FTIR nZnO vs Controls, X-ray photoelectron spectroscopy control, High-resolution TEM images, additional morphological TEM images, description of time-lapsed video. This material is available free of charge via the Internet at http://pubs.acs.org.

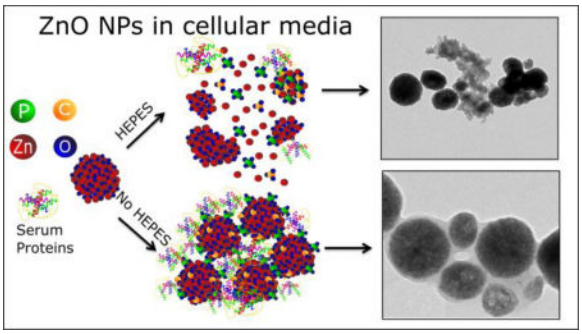

Keywords

ZnO nanoparticle; dissolution; real-time kinetics; buffer; toxicity; HEPES; media components; transformation; TEM; FT-IR; XPS

INTRODUCTION

Nanomaterials have generated much attention over the last decade due to the emergence of novel properties generally not apparent in their bulk micron-sized counterparts. These novel properties have led to applications in electronics, optics, antimicrobial materials and coatings.[1–3] Specifically, ZnO nanoparticles (nZnO) are highly produced and extensively used in commercial products such as electronics, cosmetics and sunscreens.[4–7] However, when prepared at the nanoscale size, numerous recent reports demonstrate high cytotoxicity from nZnO in various cell lines and model organisms.[8–12] The large production volume of nZnO, coupled with an incomplete understanding of what physicochemical properties contribute to their toxicity, poses a concern to the environment and public health.[13]

The mechanism of toxicity is heavily debated, with multiple factors contributing to the source of cytotoxicity. These mechanisms are generally thought to depend on physicochemical properties such as size, dissolution kinetics and retained surface species.[14–17] With such variability in nZnO properties, numerous mechanisms have been suggested including membrane disruption, generation of reactive oxygen species (ROS) and particle dissolution.[18–20] Most researchers recognize the complex nature of deciphering the exact source of cytotoxicity as multiple mechanisms occur concurrently and vary between cell lines.[21–24]

Dissolution is considered a significant contributor to the cytotoxicity of nZnO and has been the focus of numerous studies.[25–27] The dissolution properties appear to be influenced by the size, shape, defects and synthesis procedure.[28, 29] This has established the need to present detailed physicochemical characterizations of nZnO so that researchers can decipher findings and make meaningful conclusions. Studies have shown how biologically relevant species interact and affect the dissolution properties of nZnO which has further confounded the interpretations of complex dissolution studies.[26, 27, 30] Through these studies, it has been understood that particle dissolution is affected by pH, ionic strength, adsorption of complexing ligands, phosphate ion concentration and interactions with carbonates in the media.[28–32] These findings highlight the fact that the complexity of toxicity assessments

stem from more than the physicochemical properties of nZnO and requires an understanding of how media components alter their toxicity.

Dissolution studies on particle systems are often carried out by inductively coupled plasma mass spectrometry (ICP-MS), inductively coupled plasma atomic emission spectroscopy (ICP-AES) and atomic absorption spectroscopy (AAS), which are a few of the standards for quantitative analysis. However, the quantification of nanoparticle (NP) dissolution presents difficulties including the physical separation of NPs from the dissolved ionic species, insoluble precipitant formation, and achieving an equilibrium phase along with time and cost factors.[25, 26, 33, 34] In this work, we attempt to overcome some of these challenges and present simple methods using UV/vis absorbance spectra and spectrofluorometric monitoring to measure real-time dissolution kinetics of nZnO supported by ICP-MS and microscopy techniques. Taking the dissolution results into consideration, studies on cell viability were performed to determine how common buffering systems affect dissolution kinetics that impacts the structural transformation and cytotoxicity of nZnO. To our knowledge, no reports exists that address particle dissolution induced by these buffering solutions and the resulting effects that impact NP toxicity.

EXPERIMENTAL PROCEDURES

nZnO synthesis and characterization

ZnO NP samples were produced using the forced hydrolysis method as previously reported.[35] Briefly, zinc acetate was added to diethylene glycol (DEG) and the solution brought to 80° C. Nanopure water was added and the solution was heated to 150° C and held for 90 minutes. Upon cooling to room temperature, the NPs were collected by centrifuging at 41,410 × g, subsequently washed with ethanol and the pellet dried overnight at 60° C. ZnO NPs where characterized using X-ray diffraction (XRD), transmission electron microscopy (TEM), dynamic light scattering (DLS), X-ray photoelectron spectroscopy (XPS), and Fourier transformed infrared spectroscopy (FT-IR). XRD spectra were collected using a Rigaku Miniflex 600 X-ray diffractometer and the crystal phase, lattice parameters and average crystalline size determined using Rigaku PDXL software version 1.8.0.3. NP size distributions were obtained using randomly selected particles in images obtained from a JEOL JEM-2100 HR analytical transmission electron microscope. DLS and zeta potential measurements were performed in nanopure water at a concentration of 1 mg/mL using a Malvern Zetasizer NanoZS.

Real-time kinetics of nZnO dissolution

Real-time dissolution kinetics measurements were performed using DLS, UV/vis spectrometry, fluorescence spectroscopy and confirmed using inductively coupled plasma mass spectrometry (ICP-MS). For comparison and consistency, all NP stock solutions were made by suspending nZnO at a concentration of 2.035 mg/mL, vortex mixing and sonicating the solution for 10 minutes. An aliquot of 40 μL was added to 1.92 mL of nanopure water for a final concentration of 40.7 μg/mL (~0.5mM). All buffers used were prepared at a 0.5 M concentration (except PBS, made at 20×, and sodium bicarbonate, made at 75 mg/mL) and pH adjusted to 7.4. For each interaction study, 40 μL of each stock buffer (100 uL 20× PBS)

was added to the NP solution (2mL total solution for a 2% overall change in NP concentration) to monitor NP dissolution kinetics. The Malvern Zetasizer NanoZS was used to qualitatively assess NP dissolution kinetics in size mode by acquiring 2 runs with 5 second run durations, totaling 180 runs with a 10 seconds pause in-between.

Fluorescence spectra were collected at room temperature using a FluoroMax-4 spectrofluorometer with 4.5 mL disposable cuvettes with a working range of 285 nm to 750 nm. Fluorescence spectra were collected with multiple excitation wavelengths (310–340 nm), however 310 nm was chosen to eliminate the Raman peak, associated with water, that would convolute with the nZnO emission spectra when using higher wavelengths for excitation (see supporting information, Figure S1). Monitoring the emission peak at 368 nm yielded a linear correlation between fluorescence and concentration of nZnO (see supporting information, Figure S3). For kinetics measurements, the kinetics mode was used with 310nm/368nm ex/em with 2 nm slit width and 0.5 sec integration times. Using the linear correlation, counts per second (CPS) were converted to concentration of nZnO in solution.

Absorbance spectra were obtained at room temperature using a CARY 5000 spectrophotometer using 4.5 mL disposable cuvettes with a working wavelength range of 285 to 750 nm. Initially, full absorbance spectra were collected from 290 nm to 550 nm. A linear correlation between absorbance and concentration was also achieved and dissolution kinetics was obtained by monitoring absorbance at 368 nm in kinetics mode for consistency (see supporting information, Figure S2).

For ICP-MS studies, solutions were made by the same procedure but incubated in Ultracel-4 3k centrifugal filter units (Millipore) for 20 minutes. Solutions were then centrifuged at 4,000 × g for 10 minutes to remove any NPs and precipitates. A 0.5 mL aliquot was transferred to 24.5 mL 2% high purity nitric acid solution and analyzed by the ThermoElectron X-series II quadrupole ICP-MS for determination of total free zinc ions in solution.

Effects of HEPES on the behavior of nZnO in biological media

To assess the role that HEPES plays on the dissolution properties and fate of nZnO in biological media, RPMI 1640 (see American Type Tissue Collection (ATTC) website for formulation) with and without 10 mM HEPES was used in these studies. To determine the amount of free zinc ions in solution, ICP-MS was employed to analyze the amount of free zinc in the media at various time points. For this study, 150 μL of 4.07 mg/mL ZnO NPs was added to 15 mL (40.7 μg/mL overall NP concentration) of RPMI 1640 (with and without 10 mM HEPES) in tissue culture flasks. The flasks were then moved into a cell culture incubator at 37° C and 5% CO_2 atmosphere. Two mL aliquots were taken out at various time points and transferred to Ultracel-3K centrifugal filter units and centrifuged for 10 minutes at 4,000 × g. Additional preparation for ICP-MS studies were performed as described above.

nZnO and free zinc have been shown to form precipitates in media containing sodium bicarbonate and phosphates. In order to determine how HEPES in the media influences the transformation of nZnO, XRD, XPS, and FT-IR were utilized to characterize NP/precipitate formation in the media. For basic control reactions, 50 mM $ZnCl_2$ was mixed in solution

containing sodium bicarbonate or PBS to form precipitant and was collected via centrifugation at 41,410 × g and subsequently analyzed by FT-IR (see supporting information, Figure S9). For media/nZnO studies, 10 mL of 4.07 mg/mL ZnO NP stock was added to 0.5 L of RPMI 1640 with and without 10 mM HEPES. The solution was shaken and incubated at room temperature. At various time points, the solution was centrifuged at 41,410 × g for 10 minutes. The pellet was washed with nanopure water and dried overnight at 60°C. For analysis, a Rigaku Miniflex 600 X-ray Diffractometer was used to obtain the XRD pattern of the powdered sample and images were obtained with a JEOL JEM-2100 HR analytical transmission electron microscope. XPS spectra were collected using a Physical Electronics Versaprobe system with a monochromated Al K_α X-ray source. The beam diameter was approximately 100 μm with 25 watts of power. For general survey scans, a pass energy of 117.5 eV was used and for higher resolution core level scans, a pass energy of 23.65 eV was utilized. Deconvolution of peaks was carried out using OriginPro 2017. FT-IR pellets were produced by grinding 1.5 mg of nZnO/precipitants with 2.000 g of KBr and pressed with 8 tons of pressure for 4 minutes. FT-IR spectra were collected using a Bruker Tensor 27 spectrometer. Deconvolution of the FT-IR peaks was performed using OPUS 7.0.129.

Cell culture and viability studies

To assess the effect that HEPES has on the cytotoxicity profiles of nZnO, the Jurkat T cell line was used as a model system. Cells were cultured in RPMI 1640 containing 10 mM HEPES and supplemented with 10% FBS (fetal bovine serum), 1% penicillin/streptomycin, and 2 mM L-glutamine per ATCC (American Type Culture Collection, Rockville, MD) recommendation. Cells were maintained in log phase and seeded at a concentration of 5×10^5 cells/mL in a 96-well plate for viability assays. A fresh stock solution of nZnO was prepared for each viability experiment by sonicating nZnO in autoclaved DI water at a concentration of 4.07 mg/mL for 10 minutes. RPMI 1640 without HEPES was then added to the stock solution (to avoid vehicle effects) to bring the final concentration to 2.035 mg/mL and subsequently sonicated for an additional 10 minutes. During the sonication step cells were concurrently plated and then treated with the nZnO stock solution immediately after sonication. Cells were then cultured for 24 hours at 37° C and 5% CO_2. For the Alamar Blue metabolic assay, Alamar Blue (10% (v/v) was added 20 hours after treatment with NPs and incubated for an additional 4 hours at 37° C and 5% CO_2. The fluorescence intensity was determined at 24 hours by a Biotek Synergy MX plate reader using excitation/emission at 530/590 nm. Flow cytometry was also employed to verify experimental results. After the 24 hour treatment period, cells were washed with PBS (phosphate buffered saline) and resuspended in FACS buffer (PBS/15% FBS/0.02% NaN_3) and stained with a FITC labeled anti-HLA ABC antibody (BD Biosciences, San Jose, CA). Cells were subsequently washed and 0.4 μg/mL propidium iodide (PI) was added to stain and detect non-viable cells using a BD FACS Caliber flow cytometer.

Confocal microscopy

Confocal microscopy was utilized in reflection mode to image the dissolution of nZnO. Briefly, 81.4 μg/mL solutions of nZnO in nanopure water were placed on Wilco well glass bottom dishes and allowed to dry overnight. Nanopure water was added prior to imaging as a

control to ensure the disappearance of NPs was due to dissolution from HEPES and not from solubility/dissolution in water. Confocal images were acquired in reflectance mode as a Z-stack/time series utilizing the α-Plan-FLUAR 100×/NA 1.45/ oil objective, an Argon (514 nm) laser as excitation source and a BP505-550 emission filter. Specifically, images with a frame size of 69.1 μm × 69.1 μm (0.14 μm pixel size) were acquired every 9.576 seconds for 30 minutes. To account for optical drift and ensure collecting the optical plane of interest, three 0.2 μm overlapping slices over a Z-range of 0.4 μm were collected. Image processing was performed with ZEN 2009 imaging software (Carl Zeiss, Inc., Thornwood, NY).

Statistical analysis

The data for Figure 9 were analyzed with a linear mixed model, with fixed effects of presence or absence of HEPES buffer, concentration, and their interaction. The date of the experiment was modeled as a random effect using compound symmetry for the correlation among outcomes run on the same date. Viability at each concentration was compared between HEPES and no HEPES, and comparisons were adjusted using the Bonferroni step-up correction to control family-wise type 1 error rate at 5%.[36]

RESULTS

ZnO nanoparticle synthesis and characterization

nZnO was synthesized by a wet chemical method using the forced hydrolysis of zinc acetate solubilized in DEG.[35] X-ray powder diffraction spectra showed the expected hexagonal wurzite crystal structure with an average crystal size of 9.0 ± 2.3 nm. The lattice parameters obtained from analysis were a=3.253 and c=5.215 and no other crystal phases were detected. TEM images in Figure 1 show large aggregates with a size range of 50–600 nm made up of small individual ZnO crystals of an average size of 9.8 ± 1.7 nm, which is consistent with XRD analysis (see supporting information, Figure S8). The high-resolution TEM (HRTEM) image (Figure 1C) demonstrates that the crystal lattice terminates at the boundary of the crystals, indicating no coatings or amorphous phases are present on the surface. Dynamic light scattering and electrophoretic measurements performed in nanopure water revealed an average hydrodynamic size of 345 ± 13.6 nm and zeta potential of +35.7 mV. Additional characterization information from FTIR spectra, X-ray photoelectron spectroscopy (XPS) and dissolution kinetics are discussed in subsequent sections.

Real-time dissolution kinetics

Certain media components have been shown to interact with NPs, influencing their interactions with cells due to protein corona formation, development of insoluble precipitants, and altering dissolution equilibriums.[29, 32, 37] Utilizing the newly proposed methods, numerous media components were screened to assess their effect on the dissolution properties of nZnO. Media components tested, such as glucose and various salts, had little effect on the dissolution properties in the time scale evaluated, but did affect particle aggregation and sedimentation profiles as seen in previous reports (see supporting information, Figure S4).[28, 38] Interestingly, it was found that 4-(2-hydroxyethyl)-1-piperazineethanesulfonic acid (HEPES), a common component in biological media, induces rapid dissolution of nZnO observed by UV/vis spectroscopy, fluorescence spectroscopy and

verified by ICP-MS (Figure 2). With this finding, multiple biologically relevant buffers developed by Good *et al.* were tested.[39] Many of these buffers have been used in studies of nZnO in cell culture experiments, cellular imaging and to maintain physiological pH.[25, 27, 29, 35]

The real-time dissolution kinetics of 40.7 μg/mL nZnO (highest concentration possible for linear correlation; see supplementary Fig S3) are shown in Figure 2 and demonstrate that all the buffers tested (pH = 7.4) induced rapid dissolution with various kinetics profiles. The dissolution kinetics for both absorbance and fluorescence monitoring techniques are very consistent as seen in Figure 2, and all experiments were performed in triplicate to ensure reproducibility (supporting information, Figure S6).

In order to assess the accuracy and reliability of converting the absorbance and fluorescence spectra to nZnO concentration, ICP-MS was utilized. The same reactions were completed in Ultracel-4 3k centrifugal filter units (pore size 0.1 nm) and centrifuged at 4000 × g to separate the remaining NPs from the free zinc ions. The data points were plotted over the kinetics profiles which confirmed the results obtained from the new methods, utilizing absorbance and fluorescence spectra (Figure 2).

At least 72.5% dissolution of 0.5 mM nZnO (40.7 μg/mL) was achieved from each of the buffers (10 mM; pH=7.4±0.05) within 20 minutes (Table 1). The kinetics profiles highlight the ability of these methods to monitor rapid real-time dissolution kinetics that is lost in other quantitative assessments such as ICP-MS. Additionally, these methods eliminate the need to separate the particles from the solution, reducing time and cost factors. The ability to rapidly screen how biologically and environmental relevant species impact the dissolution of nZnO will facilitate characterization and toxicity assessments.

Dynamic light scattering (DLS) was subsequently employed to qualitatively assess and confirm the dissolution of nZnO by monitoring the derived counts per second (CPS) while taking measurements in size mode. As seen in Figure 3, the number of CPS drastically reduced upon the addition of Good's buffers, while the number of CPS in PBS was maintained. In the solution containing Tricine, the system stopped collecting measurements due to insufficient signal, qualitatively confirming complete dissolution.

Confocal microscopy was utilized to visualize the dissolution of nZnO induced by the presence HEPES. No fluorescent tags were used and the images generated are due to reflection from the NP aggregates on the bottom of the well. The apparent size of the nZnO aggregates is consistent with TEM and DLS hydrodynamic size measurements. As seen in Figure 4, little to no change is detected in the integrity of the NPs in water over the ~15 minute (1000 sec) time course. However, a striking reduction in size, intensity and sharpness of the NP was seen upon the addition of HEPES (Figure 4; panel d–f). The vast majority of NPs disappeared from the images within 250 second following the addition of HEPES (see supporting information for time-lapsed video).

Morphological changes of ZnO NPs

It is important to note that the previous experiments were performed in simple solutions without salts and additional buffers such as PBS. The dynamics of nZnO in media is complex and competing events such as protein corona formation, NP agglomeration/ sedimentation and achieving dissolution equilibrium all impact the toxicity profiles of nZnO. Additionally, reports have demonstrated microstructural transformation of nZnO due to phosphate ions and have shown that free zinc ions react in media to form various zinc carbonate and phosphate precipitants.[29, 31, 40] The complex nature of cellular media affects the dissolution kinetics of nZnO and the results from the screening of numerous biological components prompted investigation into how inclusion of HEPES could potentially alter the dynamics of nZnO in cellular media.

ICP-MS was used to quantify the amount of free zinc in the media to determine any differences in dissolution kinetics from the inclusion of HEPES. nZnO was added to RPMI 1640 (with and without 10 mM HEPES) in culture flasks and placed in a cell culture incubator to mimic viability assay conditions. As seen in Figure 5, the media containing HEPES showed consistently higher levels of free zinc up to the 24 hour time point. However, at 24 hours the levels were not appreciably different. This suggests a more rapid initial dissolution of the NPs in the presence of HEPES that eventually reaches the same equilibrium regardless of media composition. Since the inclusion of HEPES in RPMI media increases the dissolution rate of nZnO, investigations into how HEPES alters the structural transformation of nZnO were performed.

X-ray diffraction (XRD) was employed to assess changes in the nZnO crystalline size and to determine if crystalline phases of zinc phosphate or zinc carbonate appear in the spectra. In media with and without HEPES, only the hexagonal wurzite crystalline phase of ZnO was detected over the 24 hour time course (see supporting information, Figure S8). However, any amorphous species formed in solution would not display a well-defined Bragg peak but broadening of the ZnO peaks were observed. During the 24 hour treatment, the apparent average crystalline size from XRD slowly reduced from ~9.3 nm to ~ 7.5 nm in both situations, but no apparent differences were noted between the samples from XRD analysis.

We have previously demonstrated that nZnO with very similar properties such as crystal size, lattice parameters and band gap have significant differences in their hydrodynamic size, zeta potential and cytotoxicity due to differences in their surface chemistry.[17] FT-IR was utilized to investigate how the surface chemistry changed and determine which species formed. The FT-IR spectra of as-prepared nZnO showed the characteristic Zn-O vibrational modes at 478 cm^{-1} (Figure 6).[17, 41] However, during the 24 hour time course, the Zn-O peak shifts down to 455 cm^{-1}, likely due to changes in the surface structure influencing the Zn-O bonds in the NPs. The two peaks at 1411 cm^{-1} and 1597 cm^{-1} are attributed to surface bound carboxylate groups retained from the zinc acetate precursor or the DEG solvent.[17] The intensity of these peaks was reduced upon addition to RPMI 1640 media and new functional groups appeared in the spectra as early as the 2 hour time point.

The emergence of the strong peak at 1050 cm^{-1} is attributed to a convolution of the PO_4^{3-} symmetric and antisymmetric stretching modes.[42, 43] The shoulder appearing at 550 cm^{-1} is

a convolution of the Zn-O stretch and a bending mode of PO_4^{3-}.[44] The shoulder appearing at 630 cm^{-1} is associated with the bending mode of PO_4^{3-} and increased in intensity over the 24 hours,[44, 45] The peak centered at 1535 cm^{-1} is due to C=O stretching, indicating carbonates and/or amide II formation derived from interactions with carbonate or proteins in the media.[46–50] Up to the 24 hour time point, nZnO shows a continual increase in peak intensity in the phosphate and carbonate/amide II regions. However, when comparing the two samples at 24 hours (Figure 7), the ratio between the area of the phosphate peaks (1050 cm^{-1}) and the area of the Zn-O modes (420,445, and 485 cm^{-1}) is higher in the media containing HEPES (4.13 vs 2.75), indicating increased dissolution and conversion to zinc phosphate.[51–55] Over the 24 hours, the O-H broad region peak increased and shifted from 3425 cm^{-1} to 3338 cm^{-1}, likely due to both the O-H region and increasing concentration of the N-H stretching regions from amide A and B bands.[49, 50] The additional peak at 1650 cm^{-1} is due to the presence of either crystalline water or more likely, the amide I mode from bound serum proteins.[42, 43, 50, 56] These results indicate the species formed are a complex mixture of nZnO, retained proteins from fetal bovine serum (FBS) in the media and insoluble precipitate formation that is likely an amorphous mixture of zinc phosphate and carbonate species

X-ray photoelectron spectroscopy (XPS) was utilized to quantify atomic concentrations of each element present, as well as verify FT-IR results. Looking at the survey spectra of nZnO/precipitants collected at 24 hours (Figure 8a), the atomic concentrations reveal that a major contribution to the amorphous species is an organic matrix likely from fetal bovine serum (FBS) proteins in the media. Additionally, looking at the ratio between the total phosphate and zinc gives atomic ratios at 2.0 (10 mM HEPES media) vs 1.65 (HEPES free media) which is very similar to results obtained from FTIR, indicating increased phosphate formations in media containing 10 mM HEPES. High resolution core level scans of the $Zn2p_{3/2}$ region demonstrate a single peak at 1021.8 eV in the as-prepared nZnO sample (Figure 8b). Once introduced to media, new zinc species become apparent, with a new peak observed with a chemical shift of +2.0 eV from the Zn-O peak (Figure 8c) indicating Zn-PO_4^{3-} bond formation (see Figure S10). These results confirm complex formations of nZnO, proteins and insoluble phosphate/carbonate precipitants.

TEM was utilized to compare the structural transformation of nZnO in both media conditions and to evaluate the integrity of the crystal lattice, formation of particle aggregates as well as amorphous species. The high-resolution TEM image in Figure 1 demonstrates that the as-prepared nZnO crystal lattice terminates at the crystal boundary with no amorphous species or coating present. In contrast, amorphous species are seen when nZnO is exposed to cellular media with or without HEPES as early as the 2 hour time point (Figure 9). From our FT-IR and XPS studies, the amorphous species formed in both cases is a mixture of proteins, zinc phosphates and carbonates. Interestingly, the morphological formation of the amorphous species is radically different due to the exclusion of HEPES in RPMI media.

The samples incubated in media containing HEPES show rapid degradation of the spherical aggregates, making the particles appear more porous. Over the 24 hour period, particle integrity is lost (Figure 9) and pieces of aggregates are seen with amorphous material spread through-out. The high-resolution TEM images (see supporting information, Figure S11)

reveal individual ZnO crystals embedded within the amorphous material. Lower magnification TEM images (Figure 9; additional figures in supporting information S11) show pieces that have broken off from the aggregates and formation of precipitates retaining aggregates/pieces with irregular morphologies.

Even though FT-IR and XPS demonstrated similar species composition in both media conditions, the transformation of nZnO was very different when HEPES was omitted from the media. Similar structures were seen in both media compositions for individual nZnO aggregates but large fractions of the samples had very different morphologies. Interestingly, instead of the rapid degradation of the aggregates seen in the presence of HEPES, the absence of HEPES allows for the amorphous species to form a matrix/corona around the particles (Figure 9). With many of particles bound together, this feature impacts their dispersion stability and rapidly settle out of solution. The porosity of the particles increases over 24 hours, however, it appears to be less dramatic when HEPES is absent with more of the spherical nature of the aggregates retained. The high-resolution TEM images (see supporting information, Figure S11) demonstrate a higher density of nZnO nanocrystals in the aggregates, and the amorphous species coat the particles instead of being randomly distributed throughout the interior of the aggregates.

Taken together, these results demonstrate that HEPES affects the dissolution and structural morphology of nZnO in complex media conditions. Inclusion of HEPES or any of the Good's buffers evaluated likely impacts particle characterization and toxicity results, and may therefore contribute to discrepancies in the literature regarding nZnO toxicity. With this is mind, we investigated how inclusion of HEPES in RPMI media impacts the cytotoxicity of nZnO.

Viability

The cytotoxic effects of nZnO on Jurkat leukemic cells have been reported by numerous groups and the source of toxicity attributed to both dissolution properties and reactive oxygen species (ROS) generation.[20, 35, 57] ROS generation may be inherent to nZnO from surface layer defects such as oxygen vacancies and elevated ROS levels have been associated with increased cytotoxicity in leukemic cell lines.[22] Direct interactions of nZnO with the mitochondrial membrane have also been shown to lead to increased ROS production.[23] Additionally, ROS can also be generated due to significant release of zinc ions, inducing mitochondrial membrane leakage and subsequent increases in intracellular superoxide levels, or possibly as a by-product of the cell death process itself.[20]

Dissolution-related cytotoxicity has been attributed to high extracellular free zinc ion concentrations and rapid intracellular dissolution in low pH environments such as endocytic vesicle fusion with lysosomes.[10] Inclusion of HEPES causes an increase in the dissolution rate of nZnO, alters the NP surface structure and morphology, all of which could influence dispersion stability, zinc ion homeostasis and ROS generation. With this in mind, investigations were performed to understand what influence the inclusion of HEPES has on the viability profile of Jurkat leukemic cells when challenged with nZnO.

Cells were treated with nZnO for 24 hours and viability determined using both flow cytometry and the Alamar Blue assay. Zinc chloride was used as a control to assess the toxicity of free zinc in the media. The Alamar Blue assay assesses the viability of live cells based on their ability to metabolically convert resazurin into a fluorescent signal. Significant changes ($p<0.001$) in viability were observed due to the exclusion of HEPES from the media (Figure 10). This could be attributed to potentially three different characteristics: i) a more rapid release of free zinc ions into the media when HEPES is present, ii) differences in surface structure/chemistry affecting ROS production and iii) increased sedimentation of the NPs when bound together by the complex matrix when excluding HEPES. The toxicity profile of the zinc chloride control was similar in trend to cells treated with nZnO in RPMI/HEPES media. This suggests that the initially higher free zinc concentration due to the inclusion of HEPES may be a significant contributor to the toxicity mechanism.

In order to verify the experimental results, viability was also determined by the uptake of propidium iodide (PI) using flow cytometry. In contrast to the Alamar Blue assay, the uptake of PI labels late apoptotic/necrotic cells by intercalating between DNA base pairs when membrane integrity is lost, thus analysis is based upon the number of dead cells in the population. A significant difference ($p<0.001$ for 3 conc.; $p< 0.05$ for 1 conc.) in the viability of Jurkat cells was observed between the two media types (Figure 10). The zinc chloride control again had a similar toxicity profile when compared to the media containing HEPES, however, at higher concentrations the zinc chloride appears more toxic. Assuming dissolution is the key driver of toxicity, this is expected since the free zinc concentration doesn’t reach equilibrium in nZnO treated media until at least the 6 hour time point (Figure 5) and nZnO crystals are still detectable after the 24 hour time course.

DISCUSSION

This paper demonstrates the ability to use simple, relatively fast and cost effective methods to quantitatively evaluate real-time dissolution kinetics of nZnO in aqueous solutions. These methods, using UV/vis or a spectrofluorometer, could potentially be adapted for use in more complex situations such as in waste water treatment studies or screenings in other biologically relevant solutions. This work also highlights that screening interactions in simple solutions can be expanded to more complex situations, leading to a better fundamental understanding of how nZnO behaves in model systems that may impact nZnO dissolution, structural transformation, dispersion and cytotoxicity profile.

The dissolution of nZnO is regarded as a significant source of cytotoxicity and a more complete understanding how non-essential media components such as Good’s buffers contribute to the dissolution kinetics may help in deciphering reports on nZnO toxicity. Good’s buffers are used extensively in biological studies to maintain physiological pH and have been reported to be used in characterizations studies such as in imaging buffers. The high level of dissolution induced by these buffers may impact results and evaluations at all levels of nZnO assessments and the impact of utilizing Good’s buffers as a buffering system needs to be considered prior to use.

The structural and chemical transformation of nZnO has been shown to be influenced by the concentration of carbonates and phosphates in solution.[29, 31] Here we demonstrate that excluding HEPES from the media significantly alters these transformations. From basic chemical assessments it appeared that there were modest changes in the dynamics of converting nZnO into zinc phosphate and zinc carbonate. However, the matrix formation that appeared in HEPES-free media suggests that even though chemically similar, structural changes can be dramatic. These structural changes potentially alter nZnO dispersion stability, causing significant changes in their sedimentation profiles. We have previously shown how dispersion stability can greatly impact the cytotoxic profile of nZnO.[58] Understanding the transformation of nZnO in *in vitro* model systems will help in further determinations on the toxicity of nZnO.

From these studies, we further demonstrated that the difference in the dissolution kinetics and transformation have significant impacts on nZnO toxicity profile in Jurkat leukemic cells. These studies highlight that the observed toxicity profile of nZnO stems from more than just the physicochemical properties of the NP. Nanoscale ZnO interactions with the environment can significantly alter their characteristics and conflicting reports on their toxicity mechanism could potentially be due to the media composition. For our future studies, we plan to investigate the use of phosphate free and HEPES free Dulbecco's Modified Eagle Medium (DMEM) in place of RPMI 1640 media for toxicity assessments to avoid potential artifacts arising from the transformation of nZnO from phosphate and increased dissolution observed from Good's buffers.

In conclusion, we have shown that a relatively simple, fast and cost effective method for screening the dissolution of nZnO can lead to a more thorough understanding of how nZnO behaves in complex conditions. These results also indicate the need for authors to ensure they list all details of the buffering systems used in published studies on nZnO due to the various media compositions required for various cell types and the wide use of Good's buffers in characterization studies such as imaging solutions.

Supplementary Material

Refer to Web version on PubMed Central for supplementary material.

Acknowledgments

Funding Sources

This research was supported in part by NSF-MRI awards (#032,233, #0722699, #0521315), NSF-RUI (DMR-0840227) and NIH (1R15CA141358-01). We also acknowledge support from the Biomolecular Research Center at Boise State University with funding from the Institutional Development Awards (IDeA) from the National Institute of General Medical Sciences of the National Institutes of Health under Grants #P20GM103408 and P20GM109095 NSF (#0619793, #0923535), the MJ Murdock Charitable Trust, and the Idaho State Board of Education.

ABBREVIATIONS

nZnO	zinc oxide nanoparticles
NP	nanoparticles

ROS	reactive oxygen species
XRD	X-ray powder diffraction
XPS	X-ray photoelectron spectroscopy
ICP-MS	inductively coupled plasma mass spectrometry
TEM	transmission electron microscopy
MOPS	3-Morpholinopropane-1-sulfonic acid
PIPES	1,4-Piperazinediethanesulfonic acid
TES	2-[[1,3-dihydroxy-2-(hydroxymethyl)propan-2-yl]amino]ethanesulfonic acid
BES	N,N-Bis-(2-hydroxyethyl)-2-aminoethanesulfonic acid
Tricine	N-(2-Hydroxy-1,1-bis(hydroxymethyl)ethyl)glycine

References

1. Kim JS, Kuk E, Yu KN, Kim JH, Park SJ, Lee HJ, Kim SH, Park YK, Park YH, Hwang CY, Kim YK, Lee YS, Jeong DH, Cho MH. Antimicrobial effects of silver nanoparticles. Nanomedicine-Nanotechnology Biology and Medicine. 2007; 3:95–101.
2. Hoye RLZ, Musselman KP, MacManus-Driscoll JL. Research Update: Doping ZnO and TiO2 for solar cells. Apl Materials. 2013; 1:11.
3. Sepulveda B, Angelome PC, Lechuga LM, Liz-Marzan LM. LSPR-based nanobiosensors. Nano Today. 2009; 4:244–251.
4. Becheri A, Durr M, Lo Nostro P, Baglioni P. Synthesis and characterization of zinc oxide nanoparticles: application to textiles as UV-absorbers. Journal of Nanoparticle Research. 2008; 10:679–689.
5. Seo YK, Kumar S, Kim GH. Analysis of Assembling ZnO Nanoparticles Into Nanogap Electrodes for Nanoscale Electronic Device Applications. Journal of Nanoscience and Nanotechnology. 2011; 11:4852–4862. [PubMed: 21770114]
6. Zvyagin AV, Zhao X, Gierden A, Sanchez W, Ross JA, Roberts MS. Imaging of zinc oxide nanoparticle penetration in human skin in vitro and in vivo. Journal of Biomedical Optics. 2008; 13:9.
7. Smijs TGM, Bouwstra JA. Focus on Skin as a Possible Port of Entry for Solid Nanoparticles and the Toxicological Impact. Journal of Biomedical Nanotechnology. 2010; 6:469–484. [PubMed: 21329042]
8. Sharma V, Shukla RK, Saxena N, Parmar D, Das M, Dhawan A. DNA damaging potential of zinc oxide nanoparticles in human epidermal cells. Toxicology Letters. 2009; 185:211–218. [PubMed: 19382294]
9. Nair S, Sasidharan A, Rani VVD, Menon D, Manzoor K, Raina S. Role of size scale of ZnO nanoparticles and microparticles on toxicity toward bacteria and osteoblast cancer cells. Journal of Materials Science-Materials in Medicine. 2009; 20:235–241. [PubMed: 18758917]
10. Muller KH, Kulkarni J, Motskin M, Goode A, Winship P, Skepper JN, Ryan MP, Porter AE. pH-Dependent Toxicity of High Aspect Ratio ZnO Nanowires in Macrophages Due to Intracellular Dissolution. Acs Nano. 2010; 4:6767–6779. [PubMed: 20949917]
11. Kumar A, Pandey AK, Singh SS, Shanker R, Dhawan A. Engineered ZnO and TiO2 nanoparticles induce oxidative stress and DNA damage leading to reduced viability of Escherichia coli. Free Radical Biology and Medicine. 2011; 51:1872–1881. [PubMed: 21920432]
12. Saptarshi SR, Duschl A, Lopata AL. Biological reactivity of zinc oxide nanoparticles with mammalian test systems: an overview. Nanomedicine. 2015; 10:2075–2092. [PubMed: 26135328]

13. Gottschalk F, Sonderer T, Scholz RW, Nowack B. Modeled Environmental Concentrations of Engineered Nanomaterials (TiO2, ZnO, Ag, CNT, Fullerenes) for Different Regions. Environmental Science & Technology. 2009; 43:9216–9222. [PubMed: 20000512]
14. Jiang JK, Oberdorster G, Biswas P. Characterization of size, surface charge, and agglomeration state of nanoparticle dispersions for toxicological studies. Journal of Nanoparticle Research. 2009; 11:77–89.
15. Yang H, Liu C, Yang DF, Zhang HS, Xi ZG. Comparative study of cytotoxicity, oxidative stress and genotoxicity induced by four typical nanomaterials: the role of particle size, shape and composition. Journal of Applied Toxicology. 2009; 29:69–78. [PubMed: 18756589]
16. Xia T, Kovochich M, Liong M, Madler L, Gilbert B, Shi HB, Yeh JI, Zink JI, Nel AE. Comparison of the Mechanism of Toxicity of Zinc Oxide and Cerium Oxide Nanoparticles Based on Dissolution and Oxidative Stress Properties. Acs Nano. 2008; 2:2121–2134. [PubMed: 19206459]
17. Punnoose A, Dodge K, Rasmussen JW, Chess J, Wingett D, Anders C. Cytotoxicity of ZnO Nanoparticles Can Be Tailored by Modifying Their Surface Structure: A Green Chemistry Approach for Safer Nanomaterials. Acs Sustainable Chemistry & Engineering. 2014; 2:1666–1673. [PubMed: 25068096]
18. Xie YP, He YP, Irwin PL, Jin T, Shi XM. Antibacterial Activity and Mechanism of Action of Zinc Oxide Nanoparticles against Campylobacter jejuni. Applied and Environmental Microbiology. 2011; 77:2325–2331. [PubMed: 21296935]
19. Akhtar MJ, Ahamed M, Kumar S, Khan MAM, Ahmad J, Alrokayan SA. Zinc oxide nanoparticles selectively induce apoptosis in human cancer cells through reactive oxygen species. International Journal of Nanomedicine. 2012; 7:845–857. [PubMed: 22393286]
20. Kao YY, Chen YC, Cheng TJ, Chiung YM, Liu PS. Zinc Oxide Nanoparticles Interfere With Zinc Ion Homeostasis to Cause Cytotoxicity. Toxicological Sciences. 2012; 125:462–472. [PubMed: 22112499]
21. Sharma V, Anderson D, Dhawan A. Zinc oxide nanoparticles induce oxidative DNA damage and ROS-triggered mitochondria mediated apoptosis in human liver cells (HepG2). Apoptosis. 2012; 17:852–870. [PubMed: 22395444]
22. Shen CC, James SA, de Jonge MD, Turney TW, Wright PFA, Feltis BN. Relating Cytotoxicity, Zinc Ions, and Reactive Oxygen in ZnO NanoparticleExposed Human Immune Cells. Toxicological Sciences. 2013; 136:120–130. [PubMed: 23997113]
23. Jeng HA, Swanson J. Toxicity of metal oxide nanoparticles in mammalian cells. Journal of Environmental Science and Health Part a-Toxic/Hazardous Substances & Environmental Engineering. 2006; 41:2699–2711.
24. Hanley C, Thurber A, Hanna C, Punnoose A, Zhang JH, Wingett DG. The Influences of Cell Type and ZnO Nanoparticle Size on Immune Cell Cytotoxicity and Cytokine Induction. Nanoscale Research Letters. 2009; 4:1409–1420. [PubMed: 20652105]
25. David CA, Galceran J, Rey-Castro C, Puy J, Companys E, Salvador J, Monne J, Wallace R, Vakourov A. Dissolution Kinetics and Solubility of ZnO Nanoparticles Followed by AGNES. Journal of Physical Chemistry C. 2012; 116:11758–11767.
26. Misra SK, Dybowska A, Berhanu D, Luoma SN, Valsami-Jones E. The complexity of nanoparticle dissolution and its importance in nanotoxicological studies. Science of the Total Environment. 2012; 438:225–232. [PubMed: 23000548]
27. Mudunkotuwa IA, Rupasinghe T, Wu CM, Grassian VH. Dissolution of ZnO Nanoparticles at Circumneutral pH: A Study of Size Effects in the Presence and Absence of Citric Acid. Langmuir. 2012; 28:396–403. [PubMed: 22122742]
28. Bian SW, Mudunkotuwa IA, Rupasinghe T, Grassian VH. Aggregation and Dissolution of 4 nm ZnO Nanoparticles in Aqueous Environments: Influence of pH, Ionic Strength, Size, and Adsorption of Humic Acid. Langmuir. 2011; 27:6059–6068. [PubMed: 21500814]
29. Mu QS, David CA, Galceran J, Rey-Castro C, Krzeminski L, Wallace R, Bamiduro F, Milne SJ, Hondow NS, Brydson R, Vizcay-Barrena G, Routledge MN, Jeuken LJC, Brown AP. Systematic Investigation of the Physicochemical Factors That Contribute to the Toxicity of ZnO Nanoparticles. Chemical Research in Toxicology. 2014; 27:558–567. [PubMed: 24575710]

30. Reed RB, Ladner DA, Higgins CP, Westerhoff P, Ranville JF. Solubility of nano-zinc oxide in environmentally and biologically important matrices. Environmental Toxicology and Chemistry. 2012; 31:93–99. [PubMed: 21994124]
31. Lv JT, Zhang SZ, Luo L, Han W, Zhang J, Yang K, Christie P. Dissolution and Microstructural Transformation of ZnO Nanoparticles under the Influence of Phosphate. Environmental Science & Technology. 2012; 46:7215–7221. [PubMed: 22651907]
32. Nel AE, Madler L, Velegol D, Xia T, Hoek EMV, Somasundaran P, Klaessig F, Castranova V, Thompson M. Understanding biophysicochemical interactions at the nano-bio interface. Nature Materials. 2009; 8:543–557. [PubMed: 19525947]
33. Herrmann R, Garcia-Garcia FJ, Reller A. Rapid degradation of zinc oxide nanoparticles by phosphate ions. Beilstein Journal of Nanotechnology. 2014; 5:2007–2015. [PubMed: 25383310]
34. Zhang JZ, He X, Zhang P, Ma YH, Ding YY, Wang ZY, Zhang ZY. Quantifying the dissolution of nanomaterials at the nano-bio interface. Science China-Chemistry. 2015; 58:761–767.
35. Hanley C, Layne J, Punnoose A, Reddy KM, Coombs I, Coombs A, Feris K, Wingett D. Preferential killing of cancer cells and activated human T cells using ZnO nanoparticles. Nanotechnology. 2008; 19:10.
36. Hochberg Y. A SHARPER BONFERRONI PROCEDURE FOR MULTIPLE TESTS OF SIGNIFICANCE. Biometrika. 1988; 75:800–802.
37. Rathnayake S, Unrine JM, Judy J, Miller AF, Rao W, Bertsch PM. Multitechnique Investigation of the pH Dependence of Phosphate Induced Transformations of ZnO Nanoparticles. Environmental Science & Technology. 2014; 48:4757–4764. [PubMed: 24693856]
38. Keller AA, Wang HT, Zhou DX, Lenihan HS, Cherr G, Cardinale BJ, Miller R, Ji ZX. Stability and Aggregation of Metal Oxide Nanoparticles in Natural Aqueous Matrices. Environmental Science & Technology. 2010; 44:1962–1967. [PubMed: 20151631]
39. Good NE, Winget GD, Winter W, Connolly TN, Izawa S, Singh RMM. HYDROGEN ION BUFFERS FOR BIOLOGICAL RESEARCH. Biochemistry. 1966; 5:467-&. [PubMed: 5942950]
40. Turney TW, Duriska MB, Jayaratne V, Elbaz A, O'Keefe SJ, Hastings AS, Piva TJ, Wright PFA, Feltis BN. Formation of Zinc-Containing Nanoparticles from Zn2+ Ions in Cell Culture Media: Implications for the Nanotoxicology of ZnO. Chemical Research in Toxicology. 2012; 25:2057–2066. [PubMed: 22978249]
41. Wahab R, Ansari SG, Kim YS, Dar MA, Shin HS. Synthesis and characterization of hydrozincite and its conversion into zinc oxide nanoparticles. Journal of Alloys and Compounds. 2008; 461:66–71.
42. Yuan AQ, Liao S, Tong ZF, Wu J, Huang ZY. Synthesis of nanoparticle zinc phosphate dihydrate by solid state reaction at room temperature and its thermochemical study. Materials Letters. 2006; 60:2110–2114.
43. Wang J, Li D, Liu J, Yang X, He J, Lu Y. One-Step Preparation and Characterization of Zinc Phosphate Nanocrystals with Modified Surface. Soft Nanoscience Letters. 2011:81–85.
44. Pawlig O, Trettin R. Synthesis and characterization of alpha-hopeite, Zn-3(Po-4)(2)center dot 4H(2)O. Materials Research Bulletin. 1999; 34:1959–1966.
45. Jung SH, Oh E, Shim D, Park DH, Cho S, Lee BR, Jeong YU, Lee KH, Jeong SH. Sonochemical Synthesis of Amorphous Zinc Phosphate Nanospheres. Bulletin of the Korean Chemical Society. 2009; 30:2280–2282.
46. Hales MC, Frost RL. Synthesis and vibrational spectroscopic characterisation of synthetic hydrozincite and smithsonite. Polyhedron. 2007; 26:4955–4962.
47. Cheng JQ, Poduska KM. A Strategy for Hydroxide Exclusion in Nanocrystalline Solid-State Metathesis Products. Nanomaterials. 2013; 3:317–324. [PubMed: 28348338]
48. Kanari N, Mishra D, Gaballah I, Dupre B. Mineral Processing Environm, E. Thermal decomposition of zinc carbonate hydroxide. Thermochimica Acta. 2004; 410:93–100.
49. Kong J, Yu S. Fourier transform infrared spectroscopic analysis of protein secondary structures. Acta Biochimica Et Biophysica Sinica. 2007; 39:549–559. [PubMed: 17687489]
50. Barth A. Infrared spectroscopy of proteins. Biochimica Et Biophysica Acta-Bioenergetics. 2007; 1767:1073–1101.

51. Sahai A, Goswami N. Structural and vibrational properties of ZnO nanoparticles synthesized by the chemical precipitation method. Physica E-Low-Dimensional Systems & Nanostructures. 2014; 58:130–137.

52. Decremps F, Pellicer-Porres J, Saitta AM, Chervin JC, Polian A. High-pressure Raman spectroscopy study of wurtzite ZnO. Physical Review B. 2002; 65:4.

53. Wang RP, Xu G, Jin P. Size dependence of electron-phonon coupling in ZnO nanowires. Physical Review B. 2004; 69:4.

54. Munoz-Hernandez G, Escobedo-Morales A, Pal U. Thermolytic Growth of ZnO Nanocrystals: Morphology Control and Optical Properties. Crystal Growth & Design. 2009; 9:297–300.

55. Verges MA, Mifsud A, Serna CJ. FORMATION OF ROD-LIKE ZINC-OXIDE MICROCRYSTALS IN HOMOGENEOUS SOLUTIONS. Journal of the Chemical Society-Faraday Transactions. 1990; 86:959–963.

56. Huang YY, He LZ, Liu W, Fan CD, Zheng WJ, Wong YS, Chen TF. Selective cellular uptake and induction of apoptosis of cancer-targeted selenium nanoparticles. Biomaterials. 2013; 34:7106–7116. [PubMed: 23800743]

57. Buerki-Thurnherr T, Xiao LS, Diener L, Arslan O, Hirsch C, Maeder-Althaus X, Grieder K, Wampfler B, Mathur S, Wick P, Krug HF. In vitro mechanistic study towards a better understanding of ZnO nanoparticle toxicity. Nanotoxicology. 2013; 7:402–416. [PubMed: 22394310]

58. Anders CB, Chess JJ, Wingett DG, Punnoose A. Serum Proteins Enhance Dispersion Stability and Influence the Cytotoxicity and Dosimetry of ZnO Nanoparticles in Suspension and Adherent Cancer Cell Models. Nanoscale Research Letters. 2015; 10:22. [PubMed: 25852320]

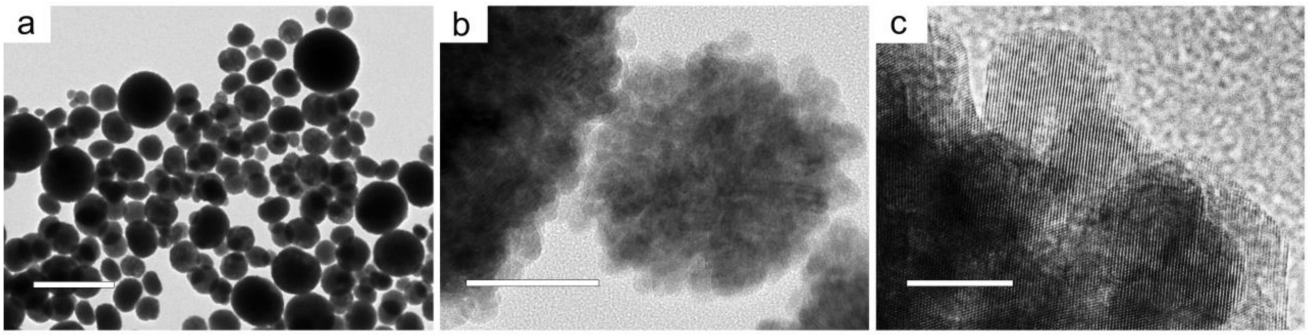

Figure 1.

(a) Scale bar: 1 μm. Low magnification image shows large spherical aggregates of ZnO with a size range of 50–600 nm. (b) Scale bar: 50 nm. Higher magnification reveals aggregates are comprised of nZnO crystals with an average size of 9.8 ± 1.7 nm. (c) Scale bar: 10 nm. High-resolution TEM image demonstrates crystal lattice termination at the crystal boundary with no amorphous structures or coatings.

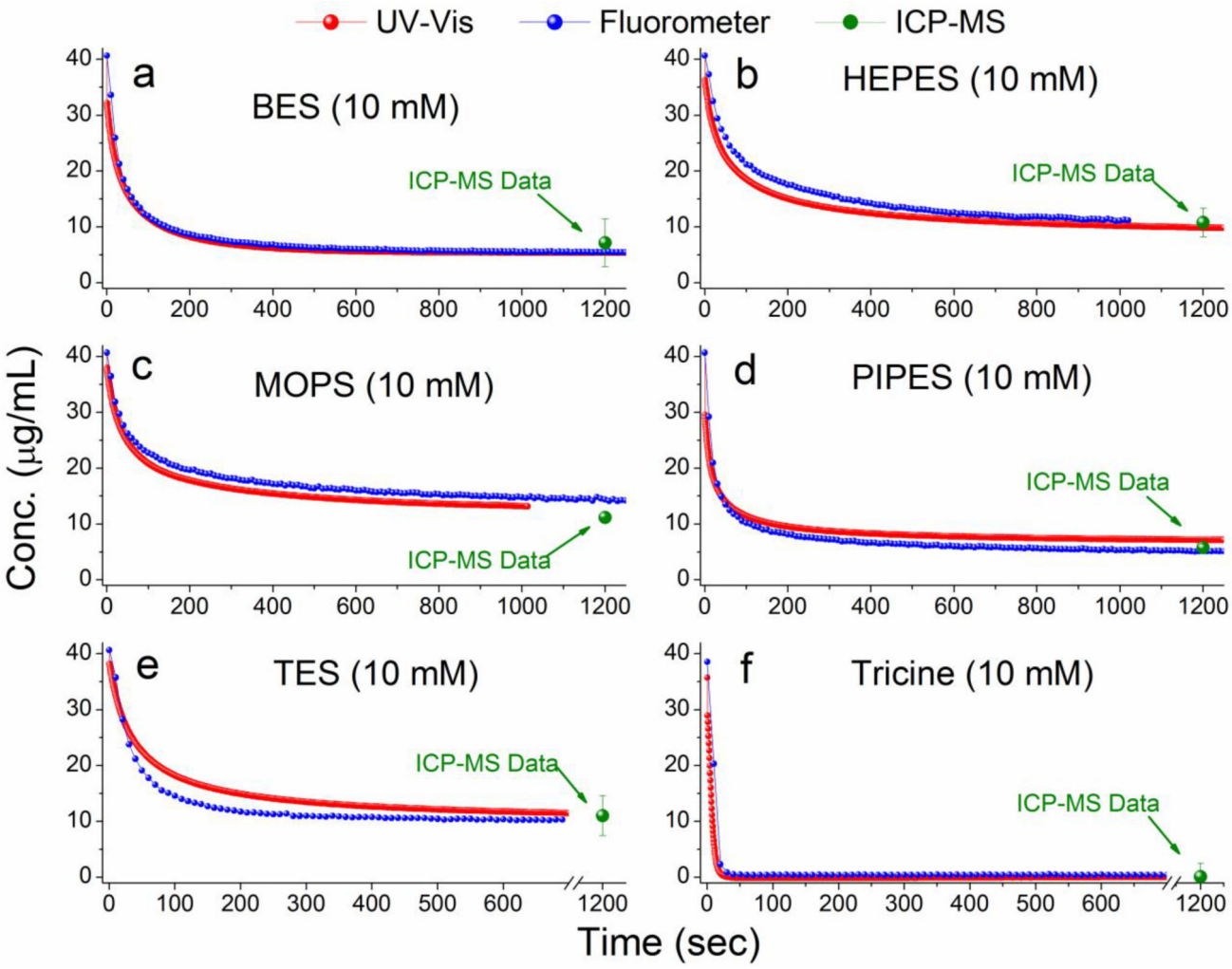

Figure 2.

(a)–(f) Real-time dissolution kinetics of 40.7 μg/mL(0.5 mM) nZnO from UV/vis spectroscopy and spectrofluorometric monitoring in various buffers developed by Good *et al.* Each buffer was prepared at a stock concentration of 500 mM and was adjusted to pH=7.4. ICP-MS data points are plotted on the kinetics profiles to demonstrate the reliability of converting spectra to quantitative concentration measurements. Measurements reveal that each of Good's buffers tested (10 mM final concentration) induced rapid dissolution of nZnO within 20 minutes.

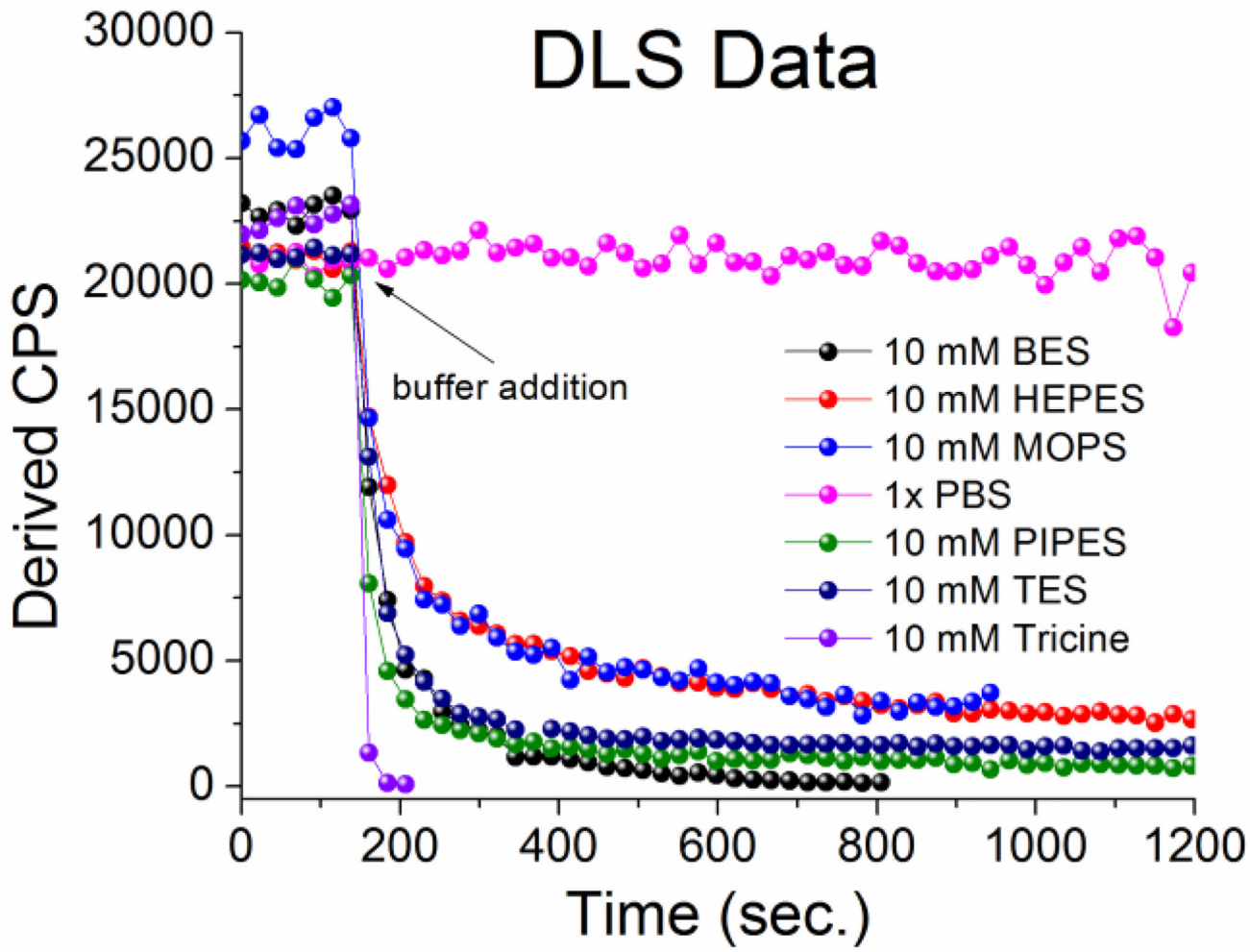

Figure 3.

A qualitative assessment of nZnO dissolution obtained from dynamic light scattering (DLS) monitored in size mode. All six Good's buffers induce rapid dissolution of nZnO as demonstrated by the fast reduction in derived counts per second (CPS).

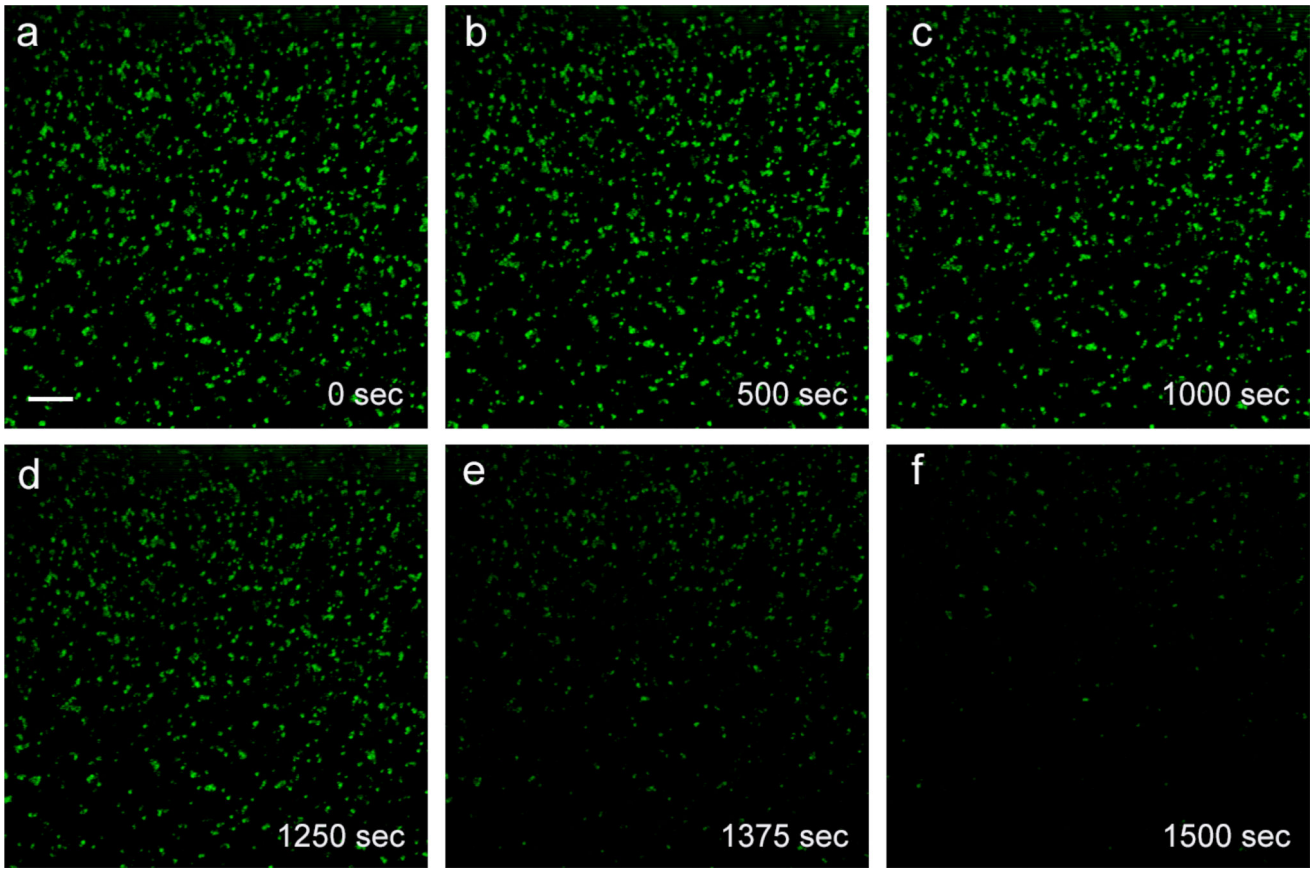

Figure 4.

Scale bar: 2 μm. A panel of nZnO confocal images obtained in reflection mode as a time series/z-stack. (a)–(c) DI water was added as a control to ensure any changes to the NPs wasn't due to solubility in water. (d)– (f) HEPES addition. nZnO quickly undergoes dissolution within the 250 second time frame, demonstrating significant dissolution by HEPES.

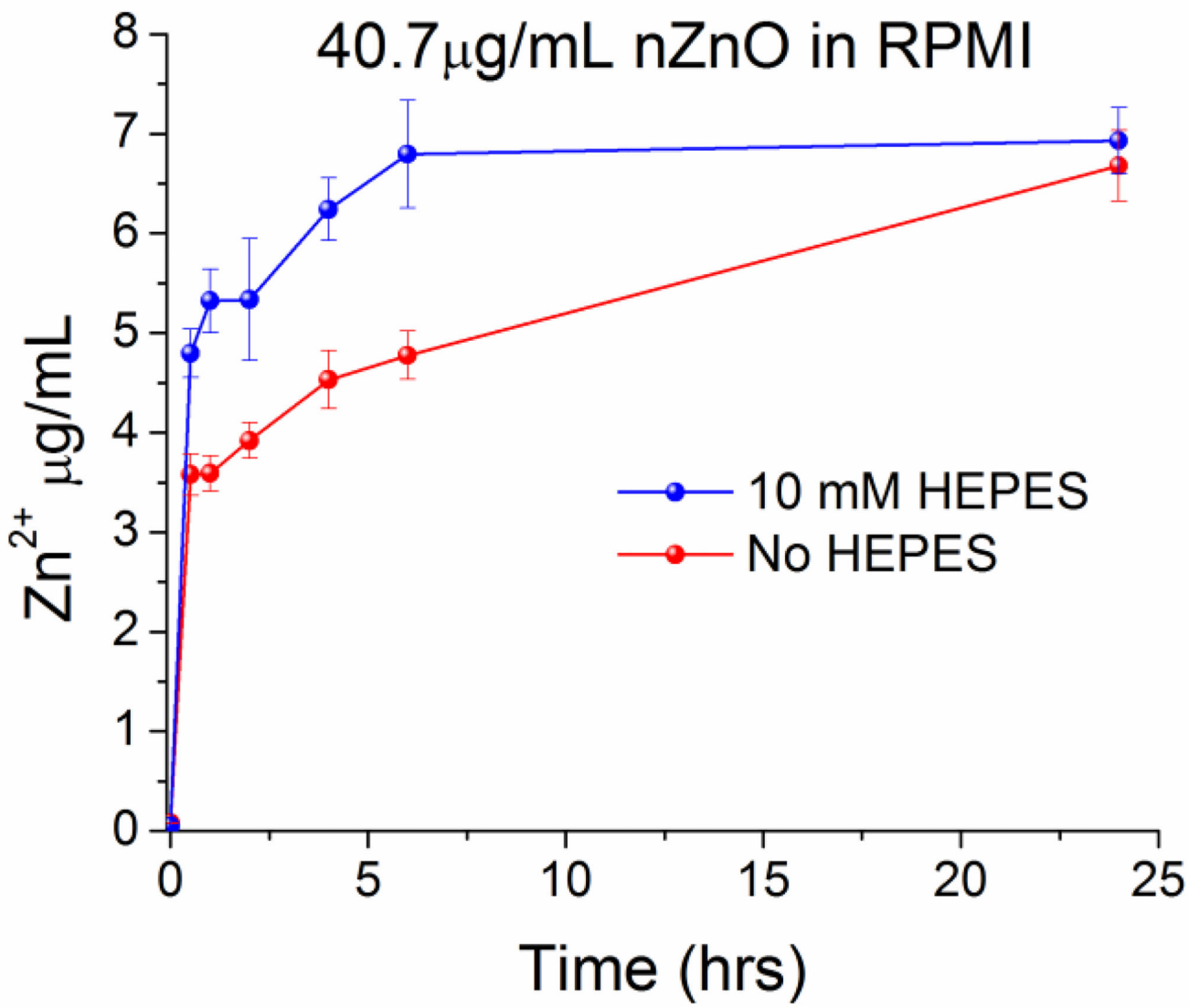

Figure 5.
ICP-MS measurements on the amount of free zinc ions from nZnO present in RPMI 1640 media with and without 10 mM HEPES over 24 hours.

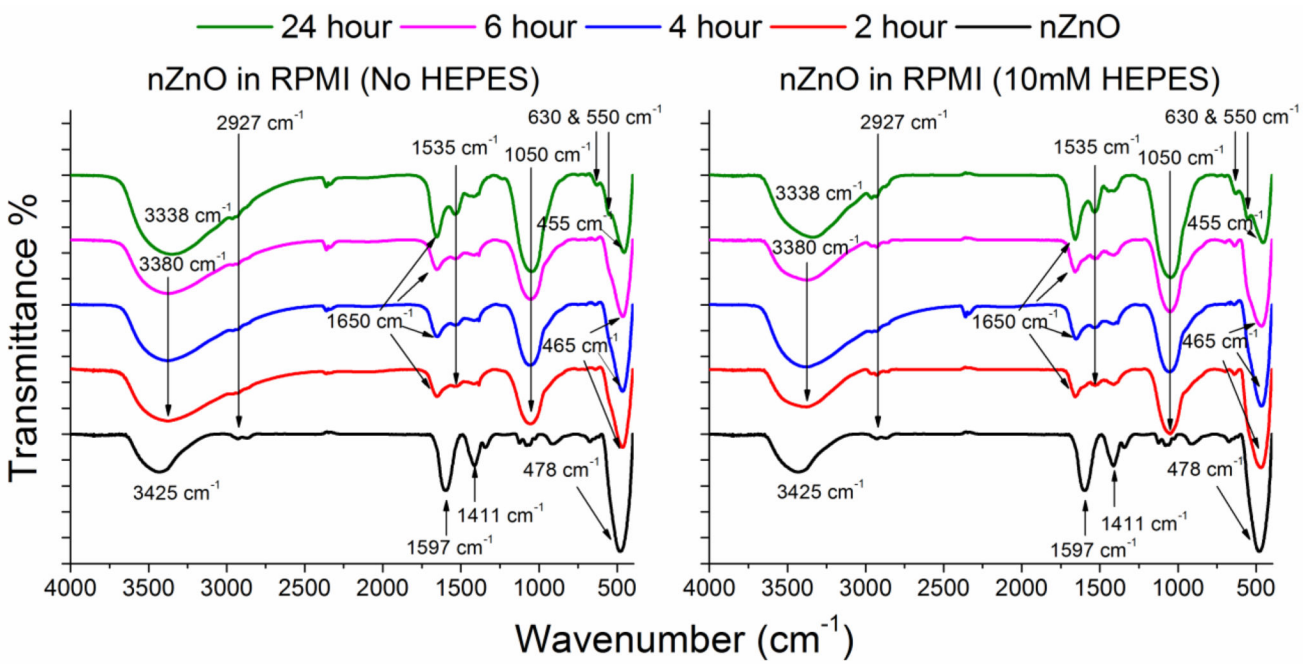

Figure 6.

FTIR spectra of as-prepared nZnO and nZnO post incubation in RPMI 1640 with (right) and without (left) 10 mM HEPES over 24 hours. The as-prepared nZnO FTIR spectra show a strong peak at 478 cm^{-1} indicative of the Zn-O modes. Other functional groups found at 1411 cm^{-1} and 1597 cm^{-1} are due to carboxylate groups retained from the zinc acetate precursor or DEG solvent. New functional groups appear upon incubation in cellular media and the peaks at 550, 630 and 1050 cm^{-1} are attributed to PO_4^{3-} stretching and bending modes. The peaks near 1535 cm^{-1} are from C=O stretching and may be from either carbonate formation or from Amide II bonds from protein corona formation. The broad O-H region shifts from 3425 cm^{-1} to 3338 cm^{-1} due to convolution of the O-H ban and new N-H stretching groups.

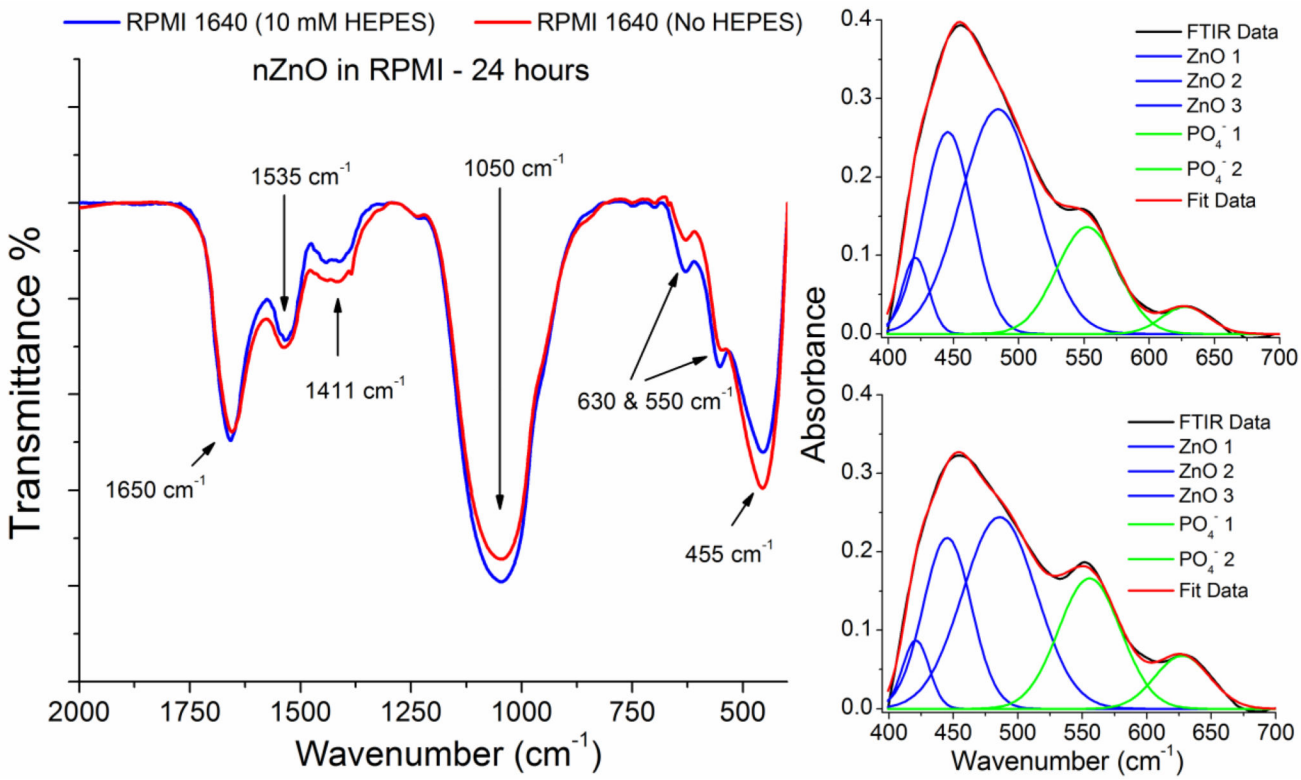

Figure 7.

(a) FTIR spectra of nZnO incubated in RPMI 1640 with (blue) and without (red) 10 mM HEPES at the 24 hour time point. The peak at 455 cm^{-1} is attributed to Zn-O modes and the broad peak at 1050 cm^{-1} is a convolution of PO_4^{3-} stretching modes. Qualitatively, the peak intensity in HEPES free media is stronger in the Zn-O modes and weaker in the phosphate stretching modes than the media containing HEPES. The deconvolution of the Zn-O modes in media containing HEPES (c) and without (b) at 24 hours was used to compare the samples. The area of the 1050 cm^{-1} phosphate peak was divided by the area of the three Zn-O peaks (420,445, and 485 cm^{-1}). A peak area ratio of 4.13 was obtained for nZnO incubated in media containing HEPES vs. a ratio of 2.75 in the media without HEPES. This demonstrates a faster conversion of nZnO to zinc phosphate in RPMI 1640 containing 10 mM HEPES.

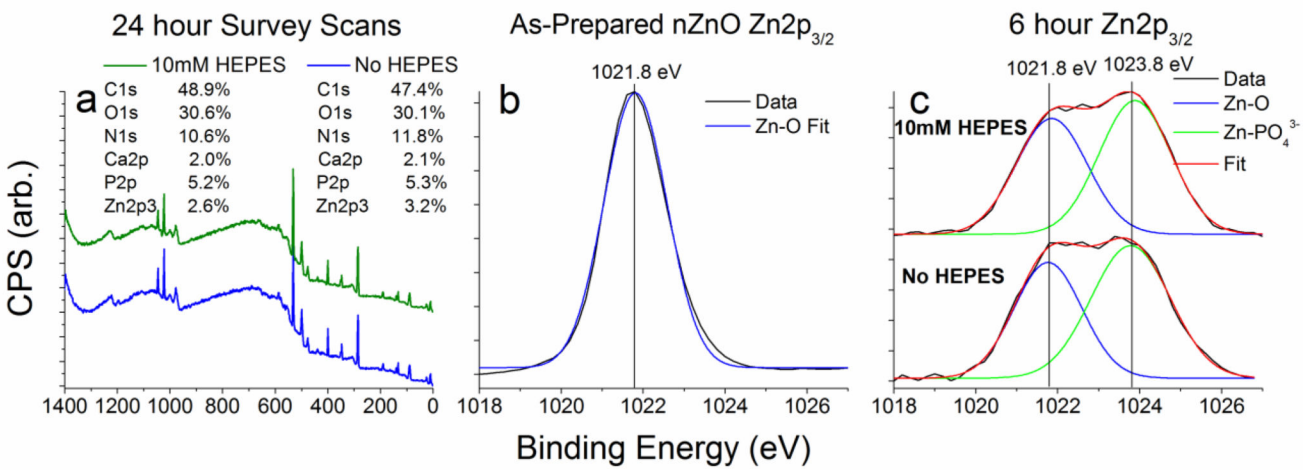

Figure 8.

XPS spectra of nZnO. (a) Survey scan of nZnO incubated in RPMI 1640 cellular media with and without 10 mM HEPES. Atomic concentrations of the various elements present are similar in both media types, however, the phosphorus to zinc ratio is different, with atomic concentration ratios of 2.0 (10 mM HEPES) and 1.65 (No HEPES). (b) The core level high resolution scan of the $Zn2p_{3/2}$ region of as-prepared nZnO demonstrates a single peak with a binding energy of 1021.8 eV. (c) A high resolution core level scan of the $Zn2p_{3/2}$ peak of nZnO incubated in cellular media for 6 hours reveals similar new zinc species present in both cases, apparent by the new peak appearing with a chemical shift of about 2 eV. XPS data verifies similar changes in media types, with a modest difference in the amount of ZnO conversion to new species.

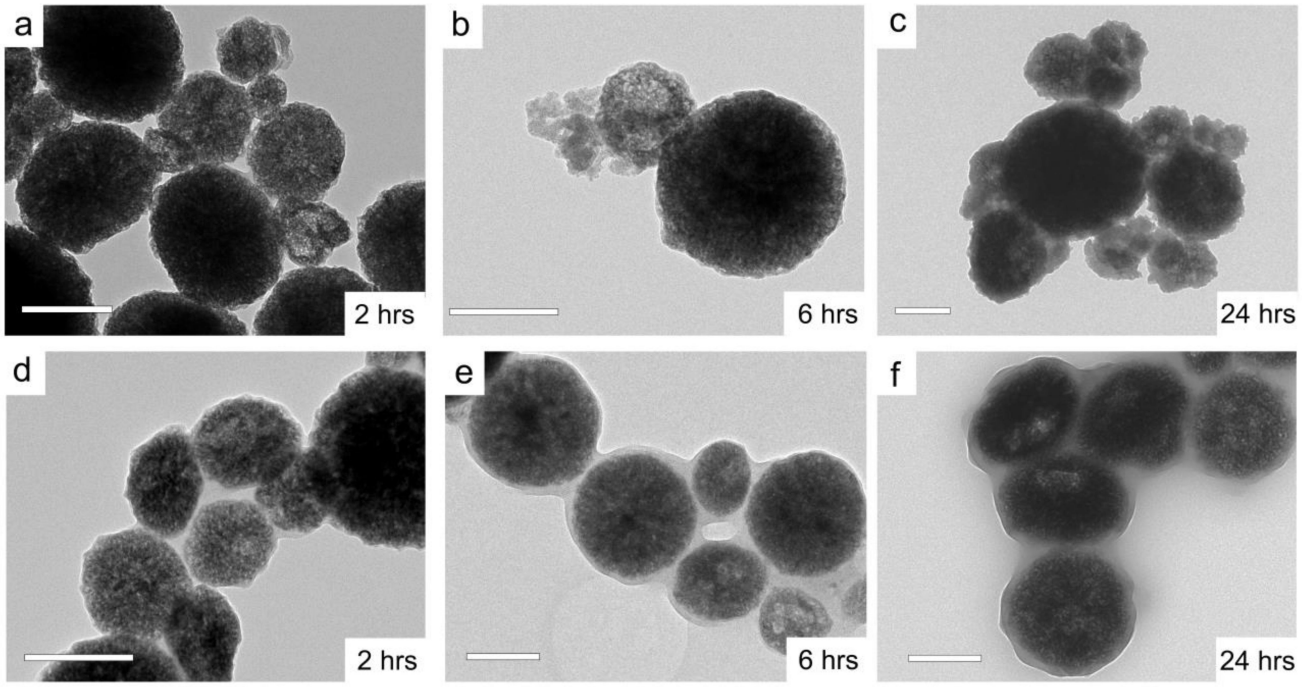

Figure 9.

(a)– (f) Scale bars: 200 nm. (a)–(c) TEM images of nZnO in RPMI containing HEPES. Over 24 hours, integrity of the particles is lost, with increasing porosity and portions of nZnO aggregates breaking off and amorphous material embedded in the particles (additional HRTEM images in supporting information). (d)– (f) TEM images of nZnO in RPMI excluding HEPES. Porosity is seen to increase over the 24 hours, however the proteins and amorphous zinc phosphate/carbonate form a matrix around the aggregates binding numerous particles together instead of embedding between the nZnO crystals in the aggregate.

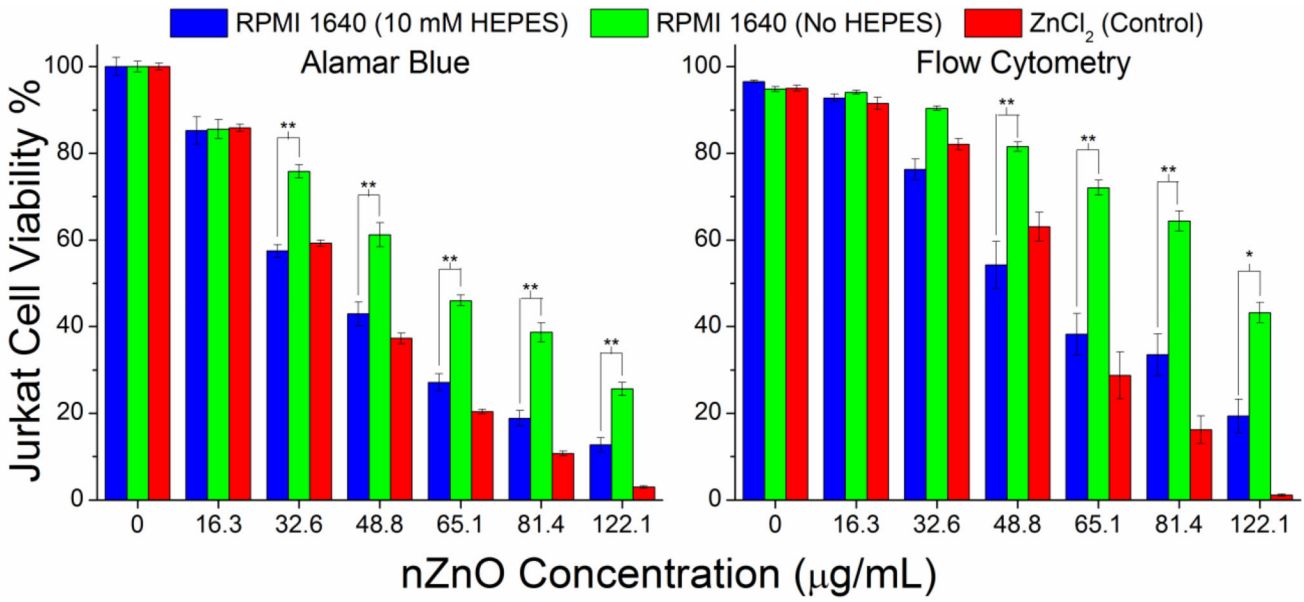

Figure 10.

nZnO toxicity on Jurkat leukemic cells at 24 hours. (Left) Alamar Blue assay demonstrating a significant difference in the toxicity of nZnO in media containing HEPES vs no HEPES. (Right) Flow cytometry analysis confirms significant changes to the viability of Jurkat cells when challenged with nZnO. (** indicates $p < 0.001$; * indicates $p < 0.05$).

Table 1

ICP-MS measurements of the dissolution of nZnO (40.7 μg/mL) in various solutions after 20 minutes. PBS and sodium bicarbonate appear to have a lower percentage of dissolved nZnO than in nanopure water. However, insoluble zinc phosphates and zinc carbonates are removed in the separation process, lowering the calculated dissolution percentage. All of Good's buffers tested (pH= 7.4) induced 72.5% or more dissolution within the 20 minute time frame.

Buffer/Media	Concentration	nZnO Dissolution %
Nanopure Water	-	4.8 ± 0.5
Phosphate Buffered Saline	1×	3.3 ± 0.3
Sodium Bicarbonate	1.5 mg/mL	1.4 ± 0.2
MOPS	10 mM	72.5 ± 0.2
TES	10 mM	72.8 ± 8.8
HEPES	10 mM	73.5 ± 6.4
BES	10 mM	82.4 ± 10.5
PIPES	10 mM	85.7 ± 1.5
Tricine	10 mM	99.6 ± 5.8